









## Spatial controls of methane uptake in upland soils across climatic and geological regions in Greenland

Ludovica D'Imperio <sup>1,2✉</sup>, Bing-Bing Li<sup>3,4,5</sup>, James M. Tiedje <sup>3,4</sup>, Youmi Oh <sup>6</sup>, Jesper Riis Christiansen<sup>2</sup>, Sebastian Kepfer-Rojas <sup>2</sup>, Andreas Westergaard-Nielsen <sup>1</sup>, Kristian Koefoed Brandt <sup>7</sup>, Peter E. Holm<sup>7</sup>, Peiyan Wang<sup>1</sup>, Per Ambus <sup>1</sup> & Bo Elberling <sup>1✉</sup>

In the Arctic, the spatiotemporal variation of net methane uptake in upland soils depends on unresolved interactive controls between edaphic and microbial factors not yet included in current models, underpinning the uncertainty of upscaling the Arctic methane budget. Here we show that upland soils in Greenland are consistent methane sinks ( $-1.83 \pm 0.19$  nmol methane  $\text{g}^{-1}$  dw  $\text{d}^{-1}$ ) across a N-S (64–83 °N) pedoclimatic transect. We demonstrate that methane oxidizers abundance, soil pH, and available soil copper are important controls on the spatial variation in methane oxidation. We revised a soil biogeochemical model with a high-resolution land classification and meteorological data for Greenland and tested it against our methane uptake measurements. The model simulated well the magnitudes of observed methane uptake but not the spatial variation across all sites. This work provides novel insights into the controls of methane uptake, which are critical for the accuracy of methane budgets.

<sup>1</sup>Center for Permafrost (CENPERM), Department of Geosciences and Natural Resource Management, University of Copenhagen, Øster Voldgade 10, DK-1350 Copenhagen, Denmark. <sup>2</sup>Section of Forest and Landscape Ecology, Department of Geosciences and Natural Resource Management, University of Copenhagen, Rolighedsvej 23, 1958 Frederiksberg C, Denmark. <sup>3</sup>Department of Plant, Soil and Microbial Sciences, Michigan State University, East Lansing, MI 48824, USA. <sup>4</sup>Center for Microbial Ecology, Michigan State University, East Lansing, MI 48824, USA. <sup>5</sup>School of Life Sciences, Anhui Agricultural University, Hefei 230036, China. <sup>6</sup>Global Monitoring Laboratory, NOAA, Boulder, CO, USA. <sup>7</sup>Department of Plant and Environmental Sciences, University of Copenhagen, Thorvaldsensvej 40, 1871 Frederiksberg, Denmark. ✉email: [ldi@ign.ku.dk](mailto:ldi@ign.ku.dk); [be@ign.ku.dk](mailto:be@ign.ku.dk)

Determining the balance between the oxidation of atmospheric methane ( $\text{CH}_4$ ) and  $\text{CH}_4$  production from Arctic ecosystems is critical for constraining the natural contribution to the global atmospheric  $\text{CH}_4$  budget. Currently, the Arctic is considered a net source of  $\text{CH}_4$  ( $15\text{--}50 \text{ Tg } \text{CH}_4 \text{ year}^{-1}$ )<sup>1</sup> with the largest biogenic contribution coming from organic carbon-rich and water-saturated soils. These ecosystems cover only 13% of the Arctic landscape<sup>2</sup>, but their high  $\text{CH}_4$  emissions have raised concern on their positive feedback on the climate at present and future warming scenario. Hence, while a large portion of research has focused on these ecosystems<sup>3</sup>, the  $\text{CH}_4$  dynamics in mineral upland soils have been overlooked in the context of the Arctic net  $\text{CH}_4$  budget. A number of field<sup>4–8</sup> and laboratory studies<sup>8–10</sup>, instead, have demonstrated that Arctic upland mineral soils are strong sinks for atmospheric  $\text{CH}_4$ . These ecosystems, covering about 87% of the Arctic<sup>2</sup> are likely to play an important, yet unquantified role in determining the net Arctic  $\text{CH}_4$  budget. In line with this empirical evidence, a recent model study<sup>11</sup> demonstrated that the activity of atmospheric methane-oxidising bacteria (MOB; methanotrophs), ubiquitous in well-aerated upland soils<sup>9,10,12,13</sup>, mitigates a large portion ( $6.2\text{--}9.5 \text{ Tg } \text{CH}_4 \text{ year}^{-1}$ )<sup>11</sup> of the current and projected increase in  $\text{CH}_4$  emissions from Arctic wetlands. The importance of soil net  $\text{CH}_4$  uptake is poorly constrained, but it is widely recognised that soil temperature, soil moisture, and substrate availability ( $\text{CH}_4$  and  $\text{O}_2$ ) are the main controls of the temporal variations of observed<sup>4,5</sup> and predicted<sup>1,2,11,14</sup> net  $\text{CH}_4$  fluxes. Only a few studies have focused on the spatial variations of net  $\text{CH}_4$  uptake in Arctic soils, and the interactive effects of soil biogeochemical and microbial community drivers are not yet identified nor included in the current models<sup>11</sup>. The soil  $\text{CH}_4$  uptake is determined by the abundance and potential (maximal) cell-specific activities of MOB, and in turn, these are regulated by the interaction with several abiotic parameters, which vary over time and space across different pedoclimatic regions. Among others, soil pH exerts a strong control on microbial community composition<sup>15,16</sup>. Recent studies have highlighted how pH shapes the methanotrophic community composition and its distribution<sup>17–19</sup> at low and high pH. Low soil pH is also linked to an increase in the concentration of available soil copper (Cu), which is an essential micro-nutrient for most organisms (especially aerobes)<sup>20</sup>. In addition, available Cu has a key regulatory function of the methane monooxygenase (MMO) enzyme, which catalyzes the first step of the  $\text{CH}_4$  oxidative reaction<sup>21,22</sup>. Although different enzymes can take part in the bacterial oxidation of methane, the available literature suggests that the Cu-containing particulate MMO (pMMO) is the most important one in terms of biogeochemical methane cycling<sup>21,22</sup>. Hence, almost all aerobic methanotrophs possess the pMMO enzyme, and expression of genes encoding other enzymes (notably soluble MMO) is often repressed in these bacteria<sup>21,22</sup>. Consequently, in this study, we targeted the *pmoA* gene encoding for the pMMO enzyme and used it as a proxy for the presence and abundance of aerobic  $\text{CH}_4$  oxidizers, which are considered the dominant group for soil  $\text{CH}_4$  oxidation. Pure culture studies have demonstrated how MOB's growth rate and carbon conversion efficiencies are promoted by the expression of pMMO, which in turn is regulated by available Cu<sup>22,23</sup>. However, to date, the links between the natural concentrations of available Cu, soil pH, and the presence and activity of MOB have not yet been reported. Hence, it is unclear if these factors also significantly contribute to determining the spatial variation of soil  $\text{CH}_4$  uptake, alongside soil moisture, soil temperature, and soil diffusive properties.

Specifically, there is a need to address in more detail the following key questions: which soil biotic and abiotic parameters

markedly influence the spatial variation of soil  $\text{CH}_4$  uptake in dry upland soils across different pedoclimatic regions? How are the spatial variation in soil pH and available soil Cu related to the distribution and activity of MOB?

To address these questions, during the month of July, we visited 11 upland sites covering a latitudinal transect ( $64^\circ\text{N}\text{--}83^\circ\text{N}$ ) along the coast of West and North Greenland. These areas are classified<sup>24</sup> as well-aerated barren soils or soils with scattered presence of dwarf shrubs and are representative of *ca.* 78% of the ice-free area of Greenland<sup>24</sup>, or *ca.* 1.5% of the total soil areal extension of the northern circumpolar permafrost region ( $17.8 \times 10^6 \text{ km}^2$ )<sup>2</sup>. At each site, we collected nine intact soil cores ( $100 \text{ cm}^3$ ) from the top (0–5 cm depth) and stored them at  $5^\circ\text{C}$  until further analyses. During laboratory incubations, we measured net soil  $\text{CH}_4$  uptake rates at atmospheric level ( $\sim 2 \text{ ppm } \text{CH}_4$  by volume). Subsequently, we analysed the soil edaphic properties and the abundances and diversities of both the methanotrophic and the total bacterial soil communities. A structural equation model (SEM) was used to explore relationships between edaphic and biotic factors and their interactive effects on net  $\text{CH}_4$  uptake rates. Finally, we compared the net  $\text{CH}_4$  uptake rates measured in this study to the estimates extrapolated from a revised version of the XPTM-XHAM biogeochemical model<sup>11</sup>. As data on the natural distribution of available Cu, soil pH and MOB abundance are not yet available to be implemented into the current model, we tested whether the XPTM-XHAM model<sup>11</sup> revised with a high-resolution land surface classification<sup>24</sup> and meteorological data from MAR v3.8 could simulate  $\text{CH}_4$  oxidation rates for Greenland consistent to our measured observations.

## Results and discussion

### Edaphic and environmental characteristics across latitudes.

The sampling sites (Fig. 1a and Supplementary Table 1) were chosen to include the large variation in environmental conditions with respect to climate and growing season length (Supplementary Fig. 1), net water balance (Fig. 1b), and parent material (Supplementary Table 1) found along the latitudinal transect. During the site visits, the mean air temperature was comparable across the transect ( $6.5 \pm 0.4^\circ\text{C}$ , based on monthly averages from MAR v3.8; see Supplementary Fig. 1).

The southern sites (A–F;  $<80^\circ\text{N}$ ), except site F, were characterised by a positive net water balance (Methods) during the growing season and had a soil water content (SWC) at the sampling time between 3 and 19 vol. % (Fig. 1b and Table 1). The five northernmost sites (G–K,  $>80^\circ\text{N}$ ) were the driest with a top soil water content ranging between 1 and 11 vol. % and a negative net water balance (Fig. 1b and Table 1). This agrees well with the general known pattern of a shift from net positive to net negative water balance from South to North of Greenland<sup>25</sup>. A negative water balance leads to upward water movement, higher salinity and even precipitation of salt on the surface. Accordingly, the northern sites were poorly weathered, nutrient-poor and the parent material was rich in carbonates, e.g., lime and dolomite, and created a strong alkaline environment (Fig. 1c and Table 1). Along the latitudinal transect, we observed a large variation in soil pH concomitant with the shift in net water balance and parent material (Fig. 1c;  $P = 0.004$ ). The soil pH variation spanned between pH 4.6 at site A and pH 9.0 at site I. In essence, this created two distinct geographical groups, i.e., southern sites (south of  $77^\circ\text{N}$ ;  $n = 6$ ) and northern sites (north of  $77^\circ\text{N}$ ;  $n = 5$ ). The distribution of available soil Cu did not show any significant relationship with latitude (Table 1; Methods) and is assumed to be controlled by site-specific characteristics such as parent material, soil organic matter and soil pH<sup>22</sup>.

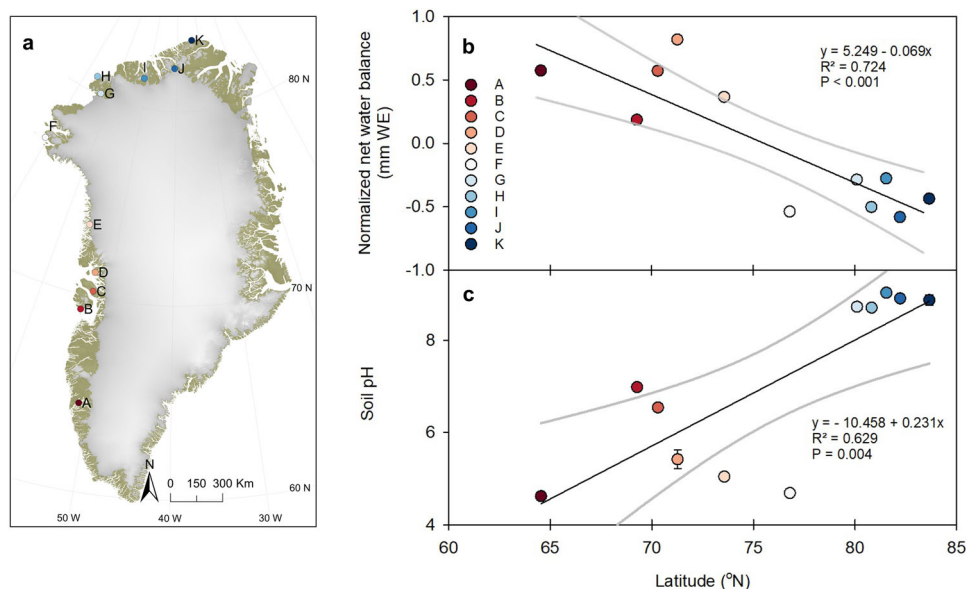


**Fig. 1** Sites location and characteristics along the latitudinal transect. In the panels: **a** Site location map, **b** linear regression (black line) and 95% confidence limits (grey lines) between normalised net water balance (cumulative for the months of June, July and August) and site locations (latitude), **c** mean soil pH ( $n = 9 \pm \text{SE}$ ). In legend, the site colour codes from south (red colour) to north (blue colour) along the latitudinal transect.

**Microbial community structure.** Microbial community structure differed significantly between sites ( $P < 0.001$ ) (Fig. 2). A total of 12011 operational taxonomic units (OTUs) belonging to 35 phyla, of which 11 accounted for  $>50\%$  of the sequences from each site were identified by amplicon sequencing of the bacterial and archaeal V4 region of the 16S rRNA gene (Methods; Supplementary Note 1 and Supplementary Fig. 2). Based on distance-based redundancy analysis (db-RDA), 33.2% of the variance in the microbial community composition was explained by the factors included (Fig. 2 and Supplementary Table 2). In particular, soil pH (Mantel test:  $r = 0.81$ ,  $P = 0.001$ ) displayed the strongest association with community dissimilarities, which is consistent with other studies<sup>16,26</sup> including high latitudes<sup>27,28</sup>. This was also observed in the microbial distribution across our latitudinal transect, which was strongly shaped by soil pH and clustered in two distinct groups corresponding to the southern and northern regions (Fig. 2).

Within the southern sites (A–F,  $<80^\circ\text{N}$ ), the same set of parameters explained the observed microbial community dissimilarities (Supplementary Fig. 3 and Supplementary Table 3). At the northern latitudes ( $>80^\circ\text{N}$ ), instead, soil pH (Mantel test:  $r = 0.17$ ,  $P = 0.03$ ) and EC (Mantel test:  $r = 0.34$ ,  $P = 0.001$ ) were overarching factors across sites (Supplementary Table 4). At these sites, the negative water balance, the site-specific geological characteristics (Supplementary Table 1), and the proximity to the ocean led to high alkalinity and higher EC, which in turn resulted as strong controls over microbial communities' dissimilarities.

**Methane uptake and methanotrophs abundance and composition.** The intact soil cores were sealed into glass jars and incubated for 5 h at  $7^\circ\text{C}$ . During incubation, we withdrew five discrete gas samples from the jar's headspace and the changes in  $\text{CH}_4$  concentration over time were measured using an Ultra-portable Greenhouse Gas Analyser (UGGA, Los Gatos, UK).

All samples showed a consistent net  $\text{CH}_4$  uptake (here reported with a negative sign indicating a decrease in headspace concentration) with variations across and within sites (Fig. 3). The average rate per site ranged between  $-0.08 \pm 0.02 \text{ nmol } \text{CH}_4 \text{ g}^{-1} \text{ dw d}^{-1}$  at site E ( $73^\circ\text{N}$ ) and a maximum of

$-4.09 \pm 1.28 \text{ nmol } \text{CH}_4 \text{ g}^{-1} \text{ dw d}^{-1}$  at site H ( $80^\circ\text{N}$ ). The average  $\text{CH}_4$  uptake rate across all the sites ( $-1.83 \pm 0.19 \text{ nmol } \text{CH}_4 \text{ g}^{-1} \text{ dw d}^{-1}$ ) fell within the range recorded in previous incubation studies<sup>5,6,9,10</sup> focusing on comparable Greenlandic ecosystems (ca.  $1 \text{ nmol } \text{CH}_4 \text{ g}^{-1} \text{ dw d}^{-1}$  at  $7^\circ\text{C}$  and  $20\text{--}25^\circ\text{C}$ <sup>5,9</sup>;  $1.24\text{--}2.14 \text{ nmol } \text{CH}_4 \text{ g}^{-1} \text{ dw d}^{-1}$  at  $10^\circ\text{C}$ <sup>9</sup>;  $0.67 \text{ nmol } \text{CH}_4 \text{ g}^{-1} \text{ dw d}^{-1}$  at  $10^\circ\text{C}$ <sup>10</sup>). We used intact soil cores to maintain the integrity of the soil structure and minimise indirect disturbances of microbial activity during the incubations. This minimum disturbance may explain the high average rates ( $>-2.5 \text{ nmol } \text{CH}_4 \text{ g}^{-1} \text{ dw d}^{-1}$ ) observed at some sites, although this alone cannot explain the higher (2-fold of site average) rates measured at site H, which may consequently be regarded as “high” for methanotrophic activity (Fig. 3).

At each site, the qPCR-derived *pmoA* gene abundance that was used as a proxy for the presence of the MOB community significantly linked to the net  $\text{CH}_4$  uptake rates (linear regression  $R^2 = 0.564$ ;  $P = 0.005$ ), but it did not show any clear distribution with latitude and varied largely both between and within sites (Table 1). The *pmoA* gene abundance exhibited a three-order-of-magnitude range, and the average abundance across sites of  $7.5 \pm 1.7 \times 10^6 \text{ copies g}^{-1} \text{ dry sample}$  ( $n = 98 \pm \text{SE}$ ) was consistent with reported values for upland grasslands<sup>13</sup>, alpine glacier forefield<sup>29</sup>, and boreal and temperate forest soils<sup>30–32</sup>. The average 16S rRNA gene copy number was  $1.9 (\pm 0.02 \text{ SE})$  using Ribosomal Database Project (RDP) Classifier<sup>33</sup>. Considering two copies of *pmoA* per MOB genome<sup>34</sup>, MOB represented approximately  $4 \pm 2.9\%$  of the prokaryotic population along the transect (Table 1). This was positively and significantly correlated ( $r = 0.279$ ,  $P < 0.01$ ) with the relative abundance of MOB extracted from 16S rDNA sequencing data (Supplementary Fig. 4), which varied between 0.06% and 4.04%.

Diverse methanotrophic bacteria were identified based on the 16S rDNA sequencing data. Type II mainly distributed in the southern sites and Type I mainly distributed in the northern sites (Supplementary Fig. 4). We further investigated the composition of the methanotrophic community (Methods) through metagenomic analysis at six selected sites (A, B, D, H, J, K), representative of the transition in net water balance and soil pH along the gradient (Supplementary Fig. 5). Compared to the

**Table 1** Abiotic and biotic soil characteristics at each site.

| Site | Lat (°N) | SOC (%)    | C:N         | pH         | EC (dS m <sup>-1</sup> ) | SWC (vol %) | Available copper <sup>a</sup> (ng g <sup>-1</sup> dw soil) | Prokaryotic population 16S rRNA (copy nr g <sup>-1</sup> dw soil) | Methanotrophs <i>pmoA</i> (copy nr g <sup>-1</sup> dw soil) | Relative abundance of <i>pmoA</i> (%) |
|------|----------|------------|-------------|------------|--------------------------|-------------|--|---|---|---------------------------------------|
| A    | 64       | 3.4 ± 0.8  | 13.7 ± 0.7  | 4.6 ± 0.03 | 0.06 ± 0.004             | 12.0 ± 0.7  | 5.2 ± 0.5  | 5.6 × 10 <sup>8</sup> ± 1.6 × 10 <sup>8</sup>                     | 5.7 × 10 <sup>6</sup> ± 1.1 × 10 <sup>6</sup>               | 2.1 ± 3.0                             |
| B    | 69       | 1.0 ± 0.1  | 9.5 ± 0.3   | 7.0 ± 0.04 | 0.03 ± 0.001             | 17.3 ± 1.5  | 20.3 ± 1.8   | 1.4 × 10 <sup>8</sup> ± 2.3 × 10 <sup>7</sup>                     | 1.5 × 10 <sup>6</sup> ± 2.3 × 10 <sup>5</sup>               | 1.2 ± 0.6                             |
| C    | 70       | 0.2 ± 0.1  | 8.3 ± 0.6   | 6.5 ± 0.02 | 0.01 ± 0.01              | 3.6 ± 0.4   | 10.5 ± 1.8   | 1.6 × 10 <sup>7</sup> ± 3.5 × 10 <sup>6b</sup>                    | 4.3 × 10 <sup>5</sup> ± 1.4 × 10 <sup>5</sup>               | 3.5 ± 3.2b                            |
| D    | 71       | 3.1 ± 0.6  | 20.5 ± 1.3b | 5.4 ± 0.20 | 0.07 ± 0.01              | 18.9 ± 1.9  | 76.2 ± 17.0  | 7.5 × 10 <sup>8</sup> ± 1.9 × 10 <sup>8b</sup>                    | 3.2 × 10 <sup>6</sup> ± 6.4 × 10 <sup>5</sup>               | 0.5 ± 0.3                             |
| E    | 73       | 0.6 ± 0.05 | 8.0 ± 0.1   | 5.0 ± 0.04 | 0.04 ± 0.002             | 8.3 ± 0.5   | 13.4 ± 2.2   | 5.7 × 10 <sup>7</sup> ± 2.1 × 10 <sup>7b</sup>                    | 1.4 × 10 <sup>5</sup> ± 3.5 × 10 <sup>4</sup>               | 0.4 ± 0.3b                            |
| F    | 76       | 1.8 ± 0.3  | 14.4 ± 1.0  | 4.7 ± 0.05 | 0.34 ± 0.003             | 19.1 ± 1.2  | 50.5 ± 2.8   | 2.9 × 10 <sup>8</sup> ± 8.7 × 10 <sup>7b</sup>                    | 9.8 × 10 <sup>5</sup> ± 2.0 × 10 <sup>5</sup>               | 0.5 ± 0.3                             |
| G    | 80       | 0.4 ± 0.06 | 8.4 ± 1.0   | 8.7 ± 0.02 | 0.17 ± 0.02              | 6.1 ± 0.7   | 4.1 ± 0.7  | 1.0 × 10 <sup>9</sup> ± 2.4 × 10 <sup>8b</sup>                    | 9.4 × 10 <sup>5</sup> ± 1.4 × 10 <sup>5</sup>               | 1.2 ± 0.7b                            |
| H    | 80       | 0.6 ± 0.03 | 6.3 ± 0.5   | 8.7 ± 0.02 | 0.23 ± 0.02              | 3.8 ± 0.7   | 25.1 ± 3.5   | 2.2 × 10 <sup>8</sup> ± 7.1 × 10 <sup>7</sup>                     | 3.7 × 10 <sup>7</sup> ± 1.5 × 10 <sup>7b</sup>              | 3.4 ± 1.8b                            |
| I    | 81       | 0.7 ± 0.0  | 9.0 ± 0.3   | 9.0 ± 0.02 | 0.12 ± 0.01              | 8.5 ± 0.3   | 8.1 ± 1.0  | 2.2 × 10 <sup>8</sup> ± 7.1 × 10 <sup>7</sup>                     | 2.6 × 10 <sup>6</sup> ± 2.4 × 10 <sup>5</sup>               | 1.9 ± 1.0                             |
| J    | 82       | 0.8 ± 0.01 | 11.1 ± 0.2  | 8.9 ± 0.06 | 0.12 ± 0.01              | 11.0 ± 1.6  | 21.8 ± 3.8   | 3.9 × 10 <sup>8</sup> ± 7.4 × 10 <sup>7b</sup>                    | 9.0 × 10 <sup>6</sup> ± 2.9 × 10 <sup>6</sup>               | 2.5 ± 2.1b                            |
| K    | 83       | 0.4 ± 0.0  | 9.5 ± 0.3   | 8.9 ± 0.11 | 0.09 ± 0.003             | 1.1 ± 0.4   | 26.9 ± 2.8   | 5.5 × 10 <sup>8</sup> ± 1.4 × 10 <sup>8</sup>                     | 2.4 × 10 <sup>7</sup> ± 4.3 × 10 <sup>6</sup>               | 5.7 ± 2.6                             |

All the values are averages (n = 9 ± standard error, SE). The abundance of prokaryotic and methanotrophic populations is reported as gene copy number (nr) by grams of dry weight (dw) soil. <sup>a</sup>Available copper was operationally defined as total Cu measured in water extracts. <sup>b</sup>n = 8

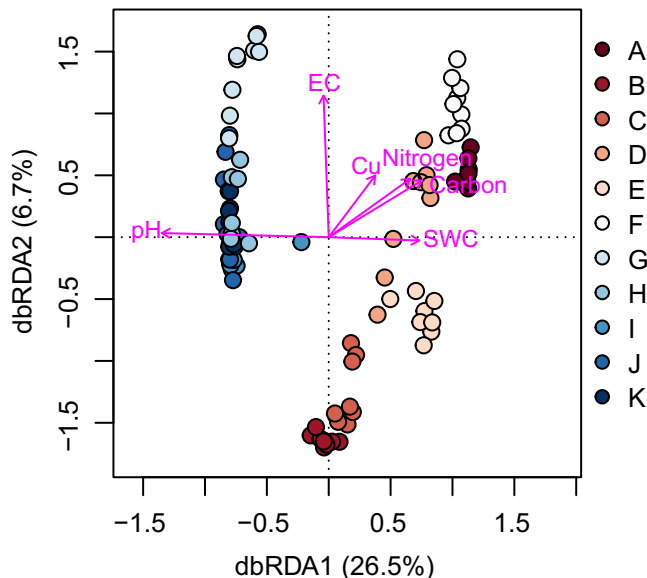


**Fig. 2** Beta-diversity of microbial community along the latitudinal transect. Distance-based redundancy analysis (db-RDA) showing the relationship between the total microbial community and the abiotic parameters (pH, EC, Cu, N, C, SWC) at the sites (n = 9). In legend, the site's colour codes from south (red colour) to north (blue colour) follow the latitudinal transect.

qPCR approach (abundance of *pmoA* genes, Table 1), three of the replicates analysed through metagenomics did not show detectable MOB (replicates B4, D2 and D5). The mismatch between the two methodologies can be explained by different detection limits, as the metagenomic analysis has higher thresholds for detection as compared to the qPCR method<sup>35</sup>. On average, 91.9% of the assembled *pmoA* genes were annotated as belonging to Alphaproteobacteria (Type IIb methanotrophs) or Gammaproteobacteria (Type Id methanotrophs) lineages ubiquitous in moist-to-dry soils and known to oxidise CH<sub>4</sub> at atmospheric concentrations<sup>17</sup>. The northern sites (H, J, K, >75°N), were dominated by the Gammaproteobacteria Upland Soil Cluster (USC)-γ (Supplementary Table 5), which has previously been found in nutrient-poor environments such as upland soils<sup>13,36</sup>, temperate grasslands<sup>19</sup>, karst caves<sup>18</sup> and desert soils<sup>37</sup>. Whereas, the MOB affiliated with the USC-α, frequently found in upland dry soils<sup>9</sup> and temperate forest soils<sup>19,31,38</sup>, represented 0–22% of the assembled *pmoA* genes among the selected northern sites (Supplementary Table 5). This result was consistent with the 16S rRNA gene sequencing result.

The rather similar CH<sub>4</sub> uptake rates measured at the southern and northern sites (e.g., sites A and K), is a surprise considering the large spatial heterogeneity of MOB diversity and abundance, which in turn could be linked to the extreme soil pH gradient measured across the latitudes (Fig. 1c), as well as to natural distributions of available soil Cu and SWC (Supplementary Fig. 6). Hence, our results point at the importance of soil pH in shaping the diversity of the MOB's community without directly affecting the soil's potential to act as a CH<sub>4</sub> sink. The MOB affiliated to USC<sub>γ</sub> have previously been found in soils with neutral to alkaline pH<sup>12,13,17,30</sup>. On the contrary, those affiliated to the USC<sub>α</sub> are known to be well-adapted to acidic soil pH<sup>19</sup>, as observed at the most southern latitudes of our transect. To date, the USC<sub>γ</sub> and USC<sub>α</sub> are uncultivated clades and there is still an incomplete understanding of their basic physiology. However, their affiliation to Type I (USC<sub>γ</sub>) and Type II (USC<sub>α</sub>) MOB suggests different carbon fixation pathways, which could lead to

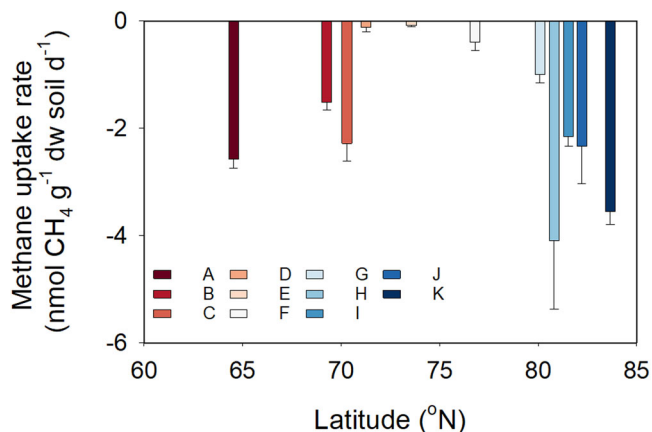


**Fig. 3 Methane uptake rates.** The soil capacity to act as a methane sink is here reported for each site along the latitudinal transect (mean  $\pm$  SE;  $n = 9$ ). In legend, the site's colour codes from south (red colour) to north (blue colour) follow the latitudinal transect.

different carbon use efficiencies, growth rates<sup>39</sup>, and cell-specific CH<sub>4</sub> oxidation capacities.

**Effects of edaphic factors on soil CH<sub>4</sub> uptake rates.** We used SEM to investigate the relationships between edaphic factors and their direct and indirect effects on the soil uptake of CH<sub>4</sub> (Methods). SEM was based on an a-priori model (Supplementary Note 2 and Supplementary Fig. 7) consisting of direct abiotic controls (pH, available Cu, soil water content and total nitrogen) on CH<sub>4</sub> uptake and their indirect effects through the abundance of MOB (Fig. 4). Our samples were collected during the summer season, with similar air temperatures across sites, and later they were incubated at 7°C and in situ water contents. Hence, we excluded potential seasonality-related effects, e.g., air temperature. Finally, we included CH<sub>4</sub> uptake rates as the main response variable. We tested this by allowing available Cu and MOB abundance to interact with soil pH. After excluding all the non-significant paths (Supplementary Table 6), the soil CH<sub>4</sub> uptake for all our sites along the latitudinal gradient was controlled by a direct and positive effect of the *pmoA* gene abundance ( $P = 0.03$ ) as well as an indirect positive effect of available Cu, through the abundance of MOB ( $P < 0.001$ ). Soil pH alone, did not show any significant relationship with the abundance of MOB, instead, it resulted in a direct and positive control on CH<sub>4</sub> uptake when interacting with available Cu ( $P = 0.001$ ). Based on our metagenomics and metabarcoding results, we observed a significant soil pH effect on the MOB community composition, but not on the total abundance of MOB. This supports the missing link between soil pH and *pmoA* abundance in the SEM, as only the MOB's abundance and not the community composition is taken into account in this analysis.

Cu solubility is known to decrease with increasing soil pH<sup>22</sup> and its low availability may constrain MOB to oxidise atmospheric CH<sub>4</sub>. On the contrary, the SEM output suggests that the soil CH<sub>4</sub> uptake rates observed along the latitudinal transect varied concordant with both soil pH and available Cu (as interaction). The site-specific microbial sensitivity to changes in Cu seems to be the driver of this complex response, which hinges on the variable background concentrations of Cu (at our sites on average low 4–76 ng g<sup>-1</sup>), soil pH, parent material and climate.

Along the observed soil pH gradient from South to North Greenland, the soil CH<sub>4</sub> uptake increased with increasing concentrations of available Cu, in particular at Northern sites with alkaline soils.

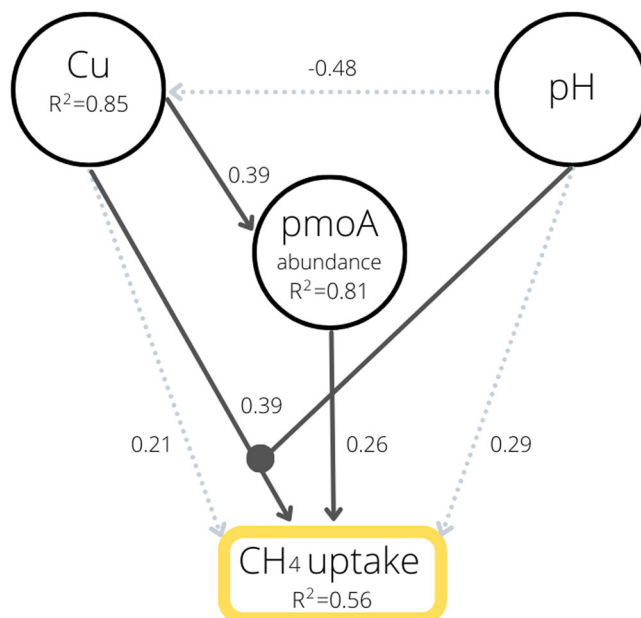


**Fig. 4 Structural equation model (SEM) showing the relationships between the variables influencing atmospheric CH<sub>4</sub> uptake rates.** For each response variable, the conditional R<sup>2</sup> is indicated. Here, available Cu is indicated as Cu. The estimates of the effects (regression coefficients) are reported next to each arrow. Solid arrows represent significant effects ( $P < 0.05$ ), whereas the dotted ones are tendencies ( $0.05 > P < 0.10$ ). The interactive effect of soil pH and available soil Cu on CH<sub>4</sub> uptake rates is indicated by a small filled circle. Fisher's C = 10.688 with  $P$  value = 0.099 and on six degrees of freedom.

Although soil hydrology is among the main factors controlling soil CH<sub>4</sub> uptake<sup>4</sup>, through its direct impact on gas diffusion as well as on the presence, distribution and activity of MOB<sup>40,41</sup>, we did not find any significant relationship between SWC and the abundance of MOB or their function. Despite very low levels of SWC (Table 1), we measured high CH<sub>4</sub> uptake rates and this was in agreement with previous in situ measurements<sup>4</sup> at dry barren soils in Disko Island (West Greenland). The SEM highlighted a significant positive correlation between Cu and SWC (across all sites), indicating that the driest sites (Northern) were also the sites with the lowest Cu availability (Table 1). However, this was not reflected in the absolute abundance of MOB (Table 1) or the net CH<sub>4</sub> uptake rates (Fig. 3).

Overall, *pmoA* abundance and the interaction of pH and available Cu, as fixed factors, explained 47% (marginal R<sup>2</sup> = 0.47) of the observed variation in CH<sub>4</sub> uptake rates. When taking into account also the spatial variation (the sampling sites were included as a random factor), the model explained up to 56% of the observed CH<sub>4</sub> uptake rates (conditional R<sup>2</sup> = 0.56).

**Methane uptake and net CH<sub>4</sub> fluxes across Greenland.** The XPTM-XHAM model, explicitly designed for High-Affinity Methanotrophs, has been employed to simulate net CH<sub>4</sub> budgets across the entire circumpolar region<sup>11</sup>. This model takes into account microbial physiology and dynamics of MOB, with optimised parameters for various vegetation types. While several soil-related factors, including pH, are considered, there is currently no function related to Cu. Here, we used a high-resolution land surface classification<sup>24</sup> and meteorological data from MAR v3.8 to drive the XPTM-XHAM model at a spatial resolution of 5-km across Greenland (59 to 82 °N; -73 to -11 °W; Methods).

To assess its suitability to simulate the spatial variability of the net CH<sub>4</sub> sink of the ice-free Greenland, we compared the

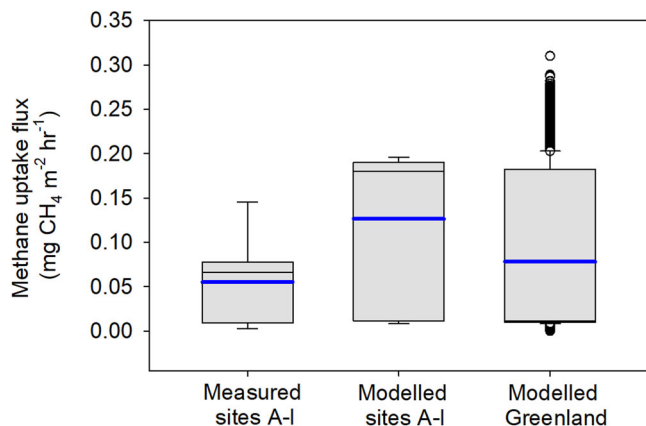


**Fig. 5** Box plot of measured and modelled methane uptake fluxes across field sites (A-I) and Greenland. All model data represent  $\text{CH}_4$  uptake fluxes during the month of July as a mean over the years 2000–2016. Inside the boxes: the blue thick line represents the average  $\text{CH}_4$  uptake ( $n = 9$  measured sites,  $n = 9$  modelled sites,  $n = 43,849$  modelled Greenland), the black line represents the median; whiskers represent the lower [ $Q1 - 1.5 \times (Q3 - Q1)$ ] and higher [ $Q3 + 1.5 \times (Q3 - Q1)$ ] limits. Outliers, values that fall outside the limits of the whiskers, are indicated by open circles.

modelled estimates of  $\text{CH}_4$  uptake to the estimates of  $\text{CH}_4$  uptake based on these laboratory incubations, after conversion to area-based units (see Methods). To ensure consistency with the period of soil samples collection, the comparison included only the modelled estimates for July (for the years 2000–2016), extrapolated from the same locations included in this study. However, sites J and K were not included, as the model did not provide any simulation above  $82^\circ\text{N}$ , which is the upper boundary of the land-cover map used.

The model results (Fig. 5) matched the magnitude of the measured  $\text{CH}_4$  uptake rates in the incubation experiment (in average:  $0.06 \pm 0.02 \text{ mg CH}_4 \text{ m}^{-2} \text{ h}^{-1}$  for the measured samples;  $0.13 \pm 0.03 \text{ mg CH}_4 \text{ m}^{-2} \text{ h}^{-1}$  for the modelled fluxes at the sites;  $0.08 \pm 0.0004 \text{ mg CH}_4 \text{ m}^{-2} \text{ h}^{-1}$  for the modelled fluxes over Greenland). However, the soil incubations represent only the top 5 cm soil with uniform temperature, whereas the model provides an estimate integrated over 1 m soil depth taking into account an increasing soil moisture and lower temperatures with depth. This is aligned with the results of depth-specific measurements suggesting that  $\text{CH}_4$  oxidation is mainly a near-surface process<sup>5</sup>.

The model was less good at capturing spatial trends observed between sites. We attribute this primarily to a lack of spatial information on soil edaphic factors related to parent material, including the vertical distribution in soil profiles of these factors as Cu availability, which cannot be captured using vegetation-specific parameters. Our incubation experiment suggests that spatial distribution of soil pH and available Cu are especially important to include in future models, as their combined effect regulates both the abundance and activities of MOB responsible for atmospheric  $\text{CH}_4$  oxidation. The current simulation of XPTEM-XHAM model estimated an annual total  $\text{CH}_4$  oxidation of  $65.6 \pm 4.9 \times 10^3 \text{ Mg CH}_4 \text{ year}^{-1}$  in dry mineral soils across Greenland (Supplementary Fig. 8). This estimate is markedly higher than the spatially extrapolated mean annual  $\text{CH}_4$  emissions ( $9.12 \pm 1.47 \times 10^3 \text{ Mg CH}_4 \text{ year}^{-1}$ ) from the XPTEM-XHAM simulations for Greenland for the years 2000–2016<sup>11</sup>. In Greenland, wetlands cover only 1.4% of the total terrestrial ecosystems, as compared to the dry upland soils covering 78% of the landscape<sup>24</sup>. The remaining area consists of dry to moist tundra and shrubs land, which have been shown to be additional but small sink areas for atmospheric methane<sup>4,5,7</sup>. Thus, with our

current best estimates of sources and sinks, the net  $\text{CH}_4$  budget reveals that Greenland is an overall sink of methane equal to  $57 [50\text{--}63] \times 10^3 \text{ Mg CH}_4 \text{ year}^{-1}$  of atmospheric  $\text{CH}_4$ , which is similar to the previous regional assessment from NE Greenland<sup>5</sup> and responsible for  $\sim 1\%$  of the estimated regional  $\text{CH}_4$  soil uptake north of  $50^\circ\text{N}$  (ca.  $5.5 \text{ Tg year}^{-1}$ )<sup>11</sup>.

## Conclusions

Our results suggest that large variations in the net soil  $\text{CH}_4$  uptake across Greenland depend on the complex interaction of MOB's abundance and composition (e.g., USC $\alpha$  and USC $\gamma$ ) and the interactions between natural concentrations of available Cu and soil pH, when not considering temporal effects of soil temperature and moisture. Therefore, we recommend that future research should focus on determining the importance of these factors on the spatial variations in  $\text{CH}_4$  uptake across different pedoclimatic regions of the Arctic beyond Greenland. Our study highlights how future models should include the interactions of these abiotic and biotic parameters, as well as other yet unidentified drivers, for a better simulation of the spatial variations in soil  $\text{CH}_4$  oxidation capacity. This, in turn, will allow a more precise estimation of the actual contribution of the dry upland ecosystems to the Arctic  $\text{CH}_4$  budget.

The net Greenland  $\text{CH}_4$  sink comprises only 1% of the net sub-Arctic and Arctic ( $60\text{--}90^\circ\text{N}$ )  $\text{CH}_4$  bottom-up budget of  $42 \text{ Tg CH}_4 \text{ year}^{-1}$ . This small contribution can be explained by the relatively small areal extent of these Greenlandic ecosystems (ca. 1.8% of the northern circumpolar permafrost region), as a consequence of their geologically young age, hence limited soil development, combined with short growing seasons and low precipitation. Nevertheless, as dry upland ecosystems cover 87% of the northern circumpolar region, our empirical and model findings highlight the need to consider these vast, well-drained areas as important contributors to the Arctic  $\text{CH}_4$  budget.

## Methods

**Sites description and soil sampling.** Eleven sites were chosen along the ice-free areas of West and North Greenland across a latitudinal transect from South ( $64^\circ\text{N}$ ) to North ( $83^\circ\text{N}$ ). Mean annual temperature varies from  $-4.8^\circ\text{C}$  in the South (sporadic permafrost) to  $-17^\circ\text{C}$  in the North (and continuous permafrost). Apart from directly affecting the activities of MOB, this temperature gradient also influences the length of the plant-growing season, and thereby the water balance (Supplementary Fig. 1). Precipitation measurements (including snow) are scarce in Greenland, but data from the Danish Meteorological Institute (DMI)<sup>24</sup> suggest  $100\text{--}150 \text{ mm year}^{-1}$  in the driest parts of North Greenland, and more than  $700 \text{ mm year}^{-1}$  in the Nuuk area. All sites were ice-covered during the last glacial maximum (21,000 years ago) and therefore represent relatively young soil types<sup>42</sup> ( $<10,000$  years old) with a weak soil development. The following 11 sites (Supplementary Table 1) were all sampled during the growing season of 2016 (mid-July to mid-August): Qoornoq (A), Disko Island (B), Nuussuaq (C), Qalatup Taserssua (D), Melville Bay (E), Nuullit (F), Cass Fjord (G), Hans Island (H), Warming Land (I), Nunataq (J), Kap Morris Jesup (K). At each site, we collected nine replicate soil cores ( $100 \text{ cm}^3$ ) from the top 0–5 cm soil depth over an area of  $100 \text{ m}^2$ . If present, we removed the top layer of gravel before sampling to ensure sampling of the portion of soil material with likely biological activity. The samples were stored at  $5^\circ\text{C}$  until further analyses, which took place within 30 days from the sampling time. Thereby, sampling represented a snapshot during the peak growing season with an air temperature variation across sites of less than 8 degrees ( $15\text{--}23^\circ\text{C}$ ) and soil

temperatures at 5 cm depth between 6 and 12 °C and a median of 7 °C.

**Climatic water balance calculations.** The water balance is critical to both the overall water content level, but also the fate of nutrients and soil pH following soil weathering and decomposition of soil organic matter. To describe quantitatively differences in summer water balance between sites, we used monthly regional climate model data from the MAR model v3.8 tuned for Greenland<sup>43</sup> with 1 km spatial resolution. The model was forced with climate data from the recently released ERA-5 reanalysis climate data. We extracted MAR data from the nearest (Haversine distance) land-based cell for each site, using the surface type mask from Bamber<sup>44</sup>. We averaged rainfall and latent heat flux data for each site during June–August in the climate normal period 1987 through 2016, and min-max-normalised rainfall and latent heat flux between sites. This allows a combined water and energy budget for the entire region with a unique high resolution, which subsequently was used for simulating CH<sub>4</sub> consumption across Greenland based on the XPTM-XHAM model, which previously has been used to simulate large-scale CH<sub>4</sub> consumption in the Arctic<sup>11</sup>.

**Laboratory incubations of intact soil cores.** We placed the intact soil cores into glass jars (365 mL) and pre-incubated them for 48 h at 7 °C. We covered the jars with perforated parafilm to avoid water loss and to ensure aerobic conditions. Afterward, we sealed each jar with a metal lid equipped with a butyl rubber septum and over-pressurised with 10 mL atmospheric air (~1.9 ppm CH<sub>4</sub>). We withdraw discrete gas samples (2 mL) with a 2 mL plastic syringe from the jar's headspace over 5 h incubation time at 7 °C. In total, five gas samples were collected from each sample after 0, 1, 2, 3, and 5 h and the CH<sub>4</sub> concentration was measured using an Ultraportable Greenhouse Gas Analyzer (UGGA, ABB - Los Gatos Research, San Jose, CA). Immediately after sampling, we fully injected the 2 mL headspace sample into a stream of dinitrogen (N<sub>2</sub>) that was fed to the inlet of the UGGA at 700 mL min<sup>-1</sup>, which matched the flow rate of the UGGA. The N<sub>2</sub> stream ensured a stable baseline where the CH<sub>4</sub> concentration was zero and consistent between every single measurement. The readings from the 2 mL samples were converted to headspace CH<sub>4</sub> concentrations in ppm based on a 4-step standard curve (1.9, 0.9, 0.45, 0.225 ppm). Gas standards were newly prepared prior to each analysis by serial dilution of a certified gas standard containing approximately ambient CH<sub>4</sub> concentration (1.9 ppm) and stored in gas-tight bags of Tedlar® film. Quality control (QC) samples containing 0.75 ppm of CH<sub>4</sub> were also prepared in a gas-tight bag and injected roughly every 26th headspace sample. Standards and QC samples were injected similarly to the headspace samples and five technical replicates were injected for each standard or QC concentration.

**Net methane uptake rate calculations.** Before CH<sub>4</sub> flux rate calculation, all the obtained CH<sub>4</sub> concentrations were quality checked by plotting them against the time of sampling. The slopes of the regressions (ppm s<sup>-1</sup>) were estimated by fitting either linear and non-linear models to the five data points (Supplementary Fig. 9). The model's choice was based on visual inspection of each regression and the best fit (*R*<sup>2</sup> value). In those samples where we observed a sharp decrease in CH<sub>4</sub> concentration during the first hour of incubation, the slope was estimated based on the first two data points to avoid an overestimation of the slope at time zero (*t* = 0). The slopes were accepted when significantly different from zero (*P* ≤ 0.05) or otherwise set to zero. The rates (ppm s<sup>-1</sup>) were converted to the net CH<sub>4</sub> uptake

rate (F<sub>CH<sub>4</sub></sub>) as nmol CH<sub>4</sub> g<sup>-1</sup> dry soil d<sup>-1</sup> using the ideal gas law as in Eq. (1).

$$F_{CH_4} = S_{CH_4} \times \frac{V}{m_{dry}} \times \frac{P}{R * T} \times 3600 \times 24 \quad (1)$$

Where *S*<sub>CH<sub>4</sub></sub> is the rate in ppm s<sup>-1</sup>, *V* is the volume of the headspace of the jar in m<sup>3</sup>, *m*<sub>dry</sub> is the dry weight of soil, *P* is the pressure in the incubation system (assumed to be 1 atm, as the effects of adding 10 mL of atm. air were considered negligible), *R* is the gas constant (m<sup>3</sup> atm K<sup>-1</sup> mol<sup>-1</sup>), *T* is the temperature in degrees Kelvin and the factor 24 × 3600 converts the rate to daily flux. The final net CH<sub>4</sub> uptake rates were reported as negative values.

**Soil chemical analyses.** After the incubations, we split the fresh intact samples for further chemical and biological analyses. Half of each fresh soil sample was freeze-dried for 48 h and the difference between their fresh and dry weight used to calculate the volumetric water content (%). The dry soil was further subsampled and a portion was finely homogenised by ball-milling and weighed (20 mg) into Ag-foil combustion capsules to measure total organic C and N contents. First, we removed the inorganic C present in the soils as described in Harris et al.<sup>45</sup>. In brief, we moistened the samples with Milli-Q water until the samples reach a water content close to the maximum water holding capacity (*ca.* 35 µL), placed in a vacuum desiccator and fumigated with 100 mL of hydrochloric acid (HCl 12 M) for 24 h. The samples were then oven-dried at 60 °C for 24 h. Finally, we estimated the contents of C and N by dry combustion using an EA1110 elemental analyser (Thermo Scientific, Bremen, Germany). Soil standards (Elemental Microanalysis, Okehampton, UK) were used for elemental analyser mass calibration.

A portion of the fresh samples (10 g) was used for cold water extraction by suspension in Milli-Q water (10 g soil: 50 mL Milli-Q H<sub>2</sub>O) and gently shaken for 1 h at room temperature. The supernatant was used to measure pH and electric conductivity (EC) with a pH meter (pH 1100 L, VWR, Germany) and a conductivity meter (CO 3100 L, VWR, Germany), respectively.

To obtain information on the availability of chemical elements, elemental composition and available copper (Cu) were determined in soil-water extracts (supernatants) generated from the remaining fresh soil samples as described in Brandt et al.<sup>46</sup> (Supplementary Note 3 and Supplementary Fig. 10). In brief, 1 g of soil was extracted with 5 mL Milli-Q water via horizontal shaking (2 h, 22 °C) and centrifugation (10,000 g, 10 min, 22 °C). Total elemental composition was determined by inductively coupled plasma-mass spectrometry (ICP-MS; Agilent 7900, Agilent Technologies, Tokyo, Japan) after digesting ground samples under pressure with aqua regia and hydrofluoric acid according to EPA 3052 (USEPA, 1996) using a closed vessel microwave-assisted system (Multiwave 3000, Anton Paar GmbH, Graz, Austria).

**Quantification of total bacterial and methanotrophs abundance.** The Powersoil DNA Extraction kit (MOBIO Laboratories, Carlsbad, CA, USA) was used to extract DNA from 0.5 g of the freeze-dried soil sample following the manufacturer's directions. The quality and concentration of the extracted DNA were measured by Nanodrop (Thermal) and Qubit kit (Life Technologies), respectively. Absolute abundances of bacteria and methanotrophs were quantified by quantitative polymerase chain reaction (qPCR). Primer sets of 515f-806rB targeting bacterial and archaeal 16S rRNA gene and 189f-682r targeting *pmoA* gene were used to assess the abundances of bacteria/archaea and methanotrophs, respectively<sup>47,48</sup>. qPCR was conducted using Power

SYBR Green PCR Master Mix (Applied Biosystems, Warrington, UK) in Applied Biosystems (ABI) 7900HT sequence detection system. A total of 10  $\mu\text{L}$  PCR reaction volume per well contained 5  $\mu\text{L}$  SYBR Green mastermix, 0.4  $\mu\text{L}$  forward and reverse primers (10  $\mu\text{M}$ ), 0.4  $\mu\text{L}$  of bovine serum albumin (BSA; 20  $\text{mg mL}^{-1}$ ), 3.3  $\mu\text{L}$  PCR grade  $\text{H}_2\text{O}$  and 0.5  $\mu\text{L}$  soil DNA with a concentration of less than 10  $\text{ng mL}^{-1}$ . Standard curves were obtained with the serial dilutions of plasmid DNA containing the target genes, which were amplified from soil DNA by 515f-806rB and 189f-682r, respectively. Then, the PCR amplified fragments were cloned using the pGEM-T vector (Promega Cor. Madison, WI USA) according to the manufacturer's instructions. Several positive clones were sequenced to make sure that correct fragments were amplified by these two primer sets. Standard PCR condition was applied for 16S rRNA gene: 10 min of polymerase activation at 95  $^{\circ}\text{C}$ , followed by 40 cycles of 15 s at 95  $^{\circ}\text{C}$ , 1 min at 60  $^{\circ}\text{C}$ . The amplification efficiencies and  $R^2$  value of primer pair of 515f-806rB were 81% and 0.996, respectively. The PCR condition for the *pmoA* gene was 10 min of polymerase activation at 95  $^{\circ}\text{C}$ , followed by 40 cycles of 30 s at 95  $^{\circ}\text{C}$ , 45 s at 57  $^{\circ}\text{C}$  and 45 s at 72  $^{\circ}\text{C}$ . The amplification efficiencies and  $R^2$  value of primer pair of 189f-682r were 85% and 0.989, respectively.

**Microbial community analysis.** Primer set 515f-806R was used to amplify the bacterial and archaeal V4 region of 16S rRNA genes<sup>49</sup>. All the amplicons were pooled together, cleaned and bidirectionally sequenced on the Illumina Miseq platform. Sequencing was performed at Research Technology Support Facility in Michigan State University, East Lansing, Michigan, United States of America. Raw sequencing reads were sorted according to barcode and assembled through the RDP modified pandaseq with low quality ( $Q$  score <25) and short reads (length <200) removed. Primers were removed through RDP SeqFilters tool<sup>50</sup>. All the 16S rRNA gene reads were classified using RDP naive Bayesian classifier after chimeras were filtered using UChime<sup>51,52</sup>. All samples of 16S rRNA gene reads were subsampled to the same sequence depth before classification, with 11395 sequences for each sample. The clean 16S rRNA gene reads were clustered by using the UPARSE pipeline of the USEARCH V8 at 97% nucleotide identity<sup>53,54</sup>. The produced OTU table and hierarchy table were further analysed using the VEGAN package in R (version 3.2.2). Bray–Curtis db-RDA was performed to illustrate the beta-diversity between treatments.

**Assembly and annotation of *pmoA* gene from shotgun metagenomic sequencing data.** Shotgun metagenomic sequencing was also performed at Research Technology Support Facility in Michigan State University. Libraries were prepared using the Illumina TruSeq Nano DNA Library Preparation Kit on a Perkin Elmer Sciclone G3 robot following the manufacturer's recommendations. Completed libraries were quality controlled and quantified using a combination of Qubit dsDNA HS and Agilent Bioanalyzer High Sensitivity DNA assays. Based on these quantifications all libraries were pooled in equimolar amounts for multiplexed sequencing. The pool was quantified using the Kapa Biosystems Illumina Library Quantification qPCR kit. This pool was then loaded onto six lanes of an Illumina HiSeq 4000 flow cell and sequenced in a  $2 \times 150$  bp paired-end format using HiSeq 4000 SBS reagents. Base calling was done by Illumina Real Time Analysis (RTA) v2.7.7 and the output of RTA was demultiplexed and converted to fastq format with Illumina Bcl2fastq v2.19.0. Raw reads in fastq files were firstly quality controlled and adaptors were trimmed by the Trimmomatic software. The assembly and annotation of the *pmoA* gene were then conducted by the target gene assembler, Xander<sup>55</sup>. The reference file of each *pmoA*

gene group was built using well-known gene sequences, protein sequences and HMMER 3.0 program, following the Xander software instructions (<https://github.com/Bingbing1110/HMMs-of-pmoA-gene>). Three *pmoA* groups (*pmoA1*, *pmoA2*, and *pmoA3*) were clustered based on a review<sup>17</sup> and recently identified methanotroph<sup>56</sup>. Therefore, the *pmoA* genes were assembled and annotated based on reference files and trimmed raw reads according to Xander's user guide. The relative abundance of each *pmoA* group was calculated based on 10,000 similarly assembled *rplB* gene sequences. The *rplB* gene is a single-copy housekeeping gene and is used to normalise target gene data to the total prokaryotic population.

**Evaluation of universal primer pair for quantification of *pmoA* gene.** The coverage of primer pair 189f-682r was evaluated by the ProbeMatch tool developed by RDP<sup>49</sup>. All retrieved *pmoA* gene sequences from metagenomic data were used as the reference database. A maximum of two mismatches was allowed. Since the *amoA* gene can be non-specifically amplified by primer pair 189f-682r, we analysed the *amoA* gene from metagenomic data and potential ammonia oxidising bacteria (AOB) from 16S rDNA sequencing data to see the specificity of 189f-682r on Greenland samples. In order to more accurately evaluate the abundances of *amoA* and *pmoA* genes, the Xander assembled *pmoA* gene and *amoA* gene sequences were reclassified by GFClassify software (<http://github.com/rdpstaff/gfclassify>), which classifies sequences into discrete categories based on their relative performance on two (or more) probabilistic models (Interpolated Context Models, ICM), in this case models built on training sets of *amoA* and *pmoA* sequences. Result showed that *amoA* gene was not assembled in most samples. Just one *amoA* contig was found. The relative abundance of AOB was very low and the specificity of primer pair 189f-682r was high on Greenland samples.

**Structural equation model.** We used multi-level path analysis or piecewise SEM (a form of structural equation modelling) to evaluate the direct and indirect relationships between soil characteristics, the abundance of methanotrophs and methane uptake rates based on 97 observations across 11 sites. Two samples (D2 and H5) were omitted due to missing data on the C/N analyses and *pmoA* abundance, respectively.

SEM is a group of statistical methods employed to test the hypothesised causal relationships between variables in multi-factorial systems<sup>57</sup>. Traditionally, SEMs are fitted using maximum likelihood methods to select parameters that represent the relationships in the observed variance-covariance matrix. Alternatively, piecewise SEM has been developed to allow the evaluation of the individual paths in the system by constructing separate models for each path. An advantage of this method is that it allows for more flexibility in the type of models that can be fitted. For instance, random effects can be included to account for the lack of independence between observations in studies involving replicated sampling in multiple sites<sup>58</sup>.

To assess the direct and interactive effects, we constructed multi-level path models and included "site" as a random effect to account for the correlation in samples taken at the same site. Available Cu and *pmoA* gene abundance were log-transformed to comply with model assumptions. Furthermore, all variables were mean centred. We did this to reduce the multicollinearity between single and interaction terms and to aid the interpretation of the interactions in our model. Complete model parameters can be found in Supplementary Table 6. We used standardised coefficients as they represent relative effect sizes. In this way, the effects of the different variables in the model are directly comparable and indicate the relative importance of each path.



The residuals of the models were visually inspected for compliance with assumptions of normality and homoscedasticity. Model fit was assessed by calculating marginal and conditional  $R^2$  for general linear mixed models<sup>59</sup>. All models were fitted with the lme4 1.1-21 package (Bates, 2015) within the piecewiseSEM 2.1.0 package<sup>58</sup> in R version 3.5.3 (R Core Team, 2019).

**Modelling approach.** The XPTEM-XHAM model based on the Terrestrial Ecosystem Model (TEM) has been used to simulate current and future methane uptake from Greenland<sup>11</sup>. The CH<sub>4</sub> dynamics module of TEM simulates CH<sub>4</sub> production, oxidation, and three transport processes—diffusion, ebullition, and plant-mediated transport—between soil and atmosphere. XPTEM-XHAM further added microbial dynamics of MOB. In this study, modelling was performed with the same parameters as described previously<sup>11</sup> but at a higher resolution (from 50- to 5-km spatial resolution). This was possible due to a high-resolution land surface classification reported for Greenland up to 82 °N<sup>24</sup>. We used meteorological inputs from the MAR v3.8 model and ran a simulation for the period from 1 January 2000 to 31 December 2016, with hourly-step for the microbial module and daily-step for other modules<sup>11</sup> with a spin-up period of 15 years. Grid cells with more than 50% of the area of ice and ocean were discarded, resulting in a total of 43,849 grid cells with 5-km resolution. Other input data, model parameters and setup remain the same as XPTEM-XHAM model<sup>11</sup>. The comparison between the model estimates and the net CH<sub>4</sub> uptake rates measured in our incubation experiment was done after harmonising all the units into area-based (mg CH<sub>4</sub> m<sup>2</sup> hr<sup>-1</sup>). The surface area of the soil core used (Ø 5 cm) for collecting the intact soil samples was used to convert our measured rates from gram of dry weight soil into m<sup>2</sup>.

**Reporting summary.** Further information on research design is available in the Nature Portfolio Reporting Summary linked to this article.

### Data availability

All raw sequencing data, including 16S rRNA gene sequencing data and shotgun sequencing data have been deposited in NCBI's Sequence Read Archive under the BioProject accession number PRJNA728249. The datasets used in this study can be accessed here <https://sid.erd.dk/sharelink/fl7ko3eRb>.

Received: 7 March 2023; Accepted: 23 November 2023;

Published online: 07 December 2023

### References

- Saunois, M. et al. The Global Methane Budget 2000–2017. *Earth Syst. Sci. Data* **12**, 1561–1623 (2020).
- Hugelius, G. et al. Estimated stocks of circumpolar permafrost carbon with quantified uncertainty ranges and identified data gaps. *Biogeosciences* **11**, 6573–6593 (2014).
- Kuhn, M. A. et al. BAWLD-CH<sub>4</sub>: a comprehensive dataset of methane fluxes from boreal and arctic ecosystems. *Earth Syst. Sci. Data* **13**, 5151–5189 (2021).
- D'Imperio, L., Nielsen, C. S., Westergaard-Nielsen, A., Michelsen, A. & Elberling, B. Methane oxidation in contrasting soil types: responses to experimental warming with implication for landscape-integrated CH<sub>4</sub> budget. *Glob. Change Biol.* **23**, 966–976 (2017).
- Jørgensen, C. J., Lund Johansen, K. M., Westergaard-Nielsen, A. & Elberling, B. Net regional methane sink in High Arctic soils of northeast Greenland. *Nat. Geosci.* **8**, 20–23 (2015).
- Voigt, C. et al. Arctic soil methane sink increases with drier conditions and higher ecosystem respiration. *Nat. Clim. Change* <https://doi.org/10.1038/s41558-023-01785-3> (2023).
- St Pierre, K. A. et al. Drivers of net methane uptake across Greenlandic dry heath tundra landscapes. *Soil Biol. Biochem.* **138**, 107605 (2019).
- Bárcena, T. G., Finster, K. W. & Yde, J. C. Spatial patterns of soil development, methane oxidation, and methanotrophic diversity along a receding glacier forefield, Southeast Greenland. *Arct. Antarct. Alp. Res.* **43**, 178–188 (2011).
- Christiansen, J. R. et al. Methane fluxes and the functional groups of methanotrophs and methanogens in a young Arctic landscape on Disko Island, West Greenland. *Biogeochemistry* **122**, 15–33 (2014).
- Lau, M. C. et al. An active atmospheric methane sink in high Arctic mineral cryosols. *ISME J.* **9**, 1880–1891 (2015).
- Oh, Y. et al. Reduced net methane emissions due to microbial methane oxidation in a warmer Arctic. *Nat. Clim. Change* **10**, 317–321 (2020).
- Knief, C., Lipski, A. & Dunfield, P. F. Diversity and activity of methanotrophic bacteria in different upland soils. *Appl. Environ. Microbiol.* **69**, 6703–6714 (2003).
- Deng, Y. et al. Upland Soil Cluster Gamma dominates methanotrophic communities in upland grassland soils. *Sci. Total Environ.* **670**, 826–836 (2019).
- Kirschke, S. et al. Three decades of global methane sources and sinks. *Nat. Geosci.* **6**, 813–823 (2013).
- Kim, J. M. et al. Soil pH and electrical conductivity are key edaphic factors shaping bacterial communities of greenhouse soils in Korea. *J. Microbiol.* **54**, 838–845 (2016).
- Fierer, N. & Jackson, R. B. The diversity and biogeography of soil bacterial communities. *Proc. Natl Acad. Sci. USA.* **103**, 626–631 (2006).
- Knief, C. Diversity and habitat preferences of cultivated and uncultivated aerobic methanotrophic bacteria evaluated based on pmoA as molecular marker. *Front. Microbiol.* **6**, 1346–1346 (2015).
- Zhao, R., Wang, H., Cheng, X., Yun, Y. & Qiu, X. Upland soil cluster  $\gamma$  dominates the methanotroph communities in the karst Heshang Cave. *FEMS Microbiol. Ecol.* **94**, <https://doi.org/10.1093/femsec/fiy192> (2018).
- Täumer, J. et al. Divergent drivers of the microbial methane sink in temperate forest and grassland soils. *Glob. Change Biol.* **27**, 929–940 (2021).
- Ridge, P. G., Zhang, Y. & Gladyshev, V. N. Comparative genomic analyses of copper transporters and Cu proteomes reveal evolutionary dynamics of copper utilization and its link to oxygen. *PLOS ONE* **3**, e1378 (2008).
- DiSpirito, A. A. et al. Methanobactin and the link between copper and bacterial methane oxidation. *Microbiol. Mol. Biol. Rev.* **80**, 387–409 (2016).
- Fru, E. C. Copper biogeochemistry: a cornerstone in aerobic methanotrophic bacterial ecology and activity? *Geomicrobiol. J.* **28**, 601–614 (2011).
- Semrau, J. D., DiSpirito, A. A. & Yoon, S. Methanotrophs and copper. *FEMS Microbiol. Rev.* **34**, 496–531 (2010).
- Karami, M. et al. A phenology-based approach to the classification of Arctic tundra ecosystems in Greenland. *ISPRS J. Photogramm. Remote Sens.* **146**, 518–529 (2018).
- Westergaard-Nielsen, A., Hansen, B. U., Elberling, B. & Abermann, J. in *Encyclopedia of World's Biomes* (eds Goldstein, M. & Della Sala, D.) 3500 (Elsevier, 2020).
- Lauber, C. L., Hamady, M., Knight, R. & Fierer, N. Pyrosequencing-based assessment of soil pH as a predictor of soil bacterial community structure at the continental scale. *Appl. Environ. Microbiol.* **75**, 5111–5120 (2009).
- Chu, H. et al. Soil bacterial diversity in the Arctic is not fundamentally different from that found in other biomes. *Environ. Microbiol.* **12**, 2998–3006 (2010).
- Ren, B. et al. Soil pH and plant diversity shape soil bacterial community structure in the active layer across the latitudinal gradients in continuous permafrost region of Northeastern China. *Sci. Rep.* **8**, 5619 (2018).
- Chiri, E., Nauer, P. A., Rainer, E.-M., Zeyer, J. & Schroth, M. H. High temporal and spatial variability of atmospheric-methane oxidation in Alpine Glacier forefield soils. *Appl. Environ. Microbiol.* **83**, <https://doi.org/10.1128/aem.01139-17> (2017).
- Kolb, S. The quest for atmospheric methane oxidizers in forest soils. *Environ. Microbiol. Rep.* **1**, 336–346 (2009).
- Kolb, S., Knief, C., Dunfield, P. F. & Conrad, R. Abundance and activity of uncultured methanotrophic bacteria involved in the consumption of atmospheric methane in two forest soils. *Environ. Microbiol.* **7**, 1150–1161 (2005).
- Bárcena, T. G. et al. Conversion of cropland to forest increases soil CH<sub>4</sub> oxidation and abundance of CH<sub>4</sub> oxidizing bacteria with stand age. *Appl. Soil Ecol.* **79**, 49–58 (2014).
- Thompson, L. R. et al. A communal catalogue reveals Earth's multiscale microbial diversity. *Nature* **551**, 457–463 (2017).
- Kolb, S., Knief, C., Stubner, S. & Conrad, R. Quantitative detection of methanotrophs in soil by novel pmoA-targeted real-time PCR assays. *Appl. Environ. Microbiol.* **69**, 2423–2429 (2003).
- Crossette, E. et al. Metagenomic quantification of genes with internal standards. *mBio* **12**, e03173–e03120 (2021).
- Martineau, C. et al. Atmospheric methane oxidizers are present and active in Canadian high Arctic soils. *FEMS Microbiol. Ecol.* **89**, 257–269 (2014).
- Angel, R. & Conrad, R. In situ measurement of methane fluxes and analysis of transcribed particulate methane monooxygenase in desert soils. *Environ. Microbiol.* **11**, 2598–2610 (2009).

38. Cai, Y., Zhou, X., Shi, L. & Jia, Z. Atmospheric methane oxidizers are dominated by upland soil cluster Alpha in 20 forest soils of China. *Microb. Ecol.* **80**, 859–871 (2020).
39. Trimmer, M. et al. Riverbed methanotrophy sustained by high carbon conversion efficiency. *ISME J.* **9**, 2304–2314 (2015).
40. Christiansen, J. R., Levy-Booth, D., Prescott, C. E. & Grayston, S. J. Microbial and environmental controls of methane fluxes along a soil moisture gradient in a Pacific coastal temperate rainforest. *Ecosystems* **19**, 1255–1270 (2016).
41. Zhang, L. et al. Distinct methanotrophic communities exist in habitats with different soil water contents. *Soil. Biol. Biochem.* **132**, 143–152 (2019).
42. Fleming, K. & Lambeck, K. Constraints on the Greenland Ice Sheet since the Last Glacial Maximum from sea-level observations and glacial-rebound models. *Quat. Sci. Rev.* **23**, 1053–1077 (2004).
43. Noël, B., Fettweis, X., van de Berg, W. J., van den Broeke, M. R. & Erpicum, M. Sensitivity of Greenland Ice Sheet surface mass balance to perturbations in sea surface temperature and sea ice cover: a study with the regional climate model MAR. *Cryosphere* **8**, 1871–1883 (2014).
44. Bamber, J. L. et al. A new bed elevation dataset for Greenland. *Cryosphere* **7**, 499–510 (2013).
45. Harris, D., Horwath, W. R. & van Kessel, C. Acid fumigation of soils to remove carbonates prior to total organic carbon or CARBON-13 isotopic analysis. *Soil Sci. Soc. Am. J.* **65**, 1853–1856 (2001).
46. Brandt, K. K., Holm, P. E. & Nybroe, O. Evidence for bioavailable copper-dissolved organic matter complexes and transiently increased copper bioavailability in manure-amended soils as determined by bioluminescent bacterial biosensors. *Environ. Sci. Technol.* **42**, 3102–3108 (2008).
47. Apprill, A., McNally, S., Parsons, R. & Weber, L. Minor revision to V4 region SSU rRNA 806R gene primer greatly increases detection of SAR11 bacterioplankton. *Aquat. Microb. Ecol.* **75**, 129–137 (2015).
48. Holmes, A. J., Costello, A., Lidstrom, M. E. & Murrell, J. C. Evidence that particulate methane monooxygenase and ammonia monooxygenase may be evolutionarily related. *FEMS Microbiol. Lett.* **132**, 203–208 (1995).
49. Kozich, J. J., Westcott, S. L., Baxter, N. T., Highlander, S. K. & Schloss, P. D. Development of a dual-index sequencing strategy and curation pipeline for analyzing amplicon sequence data on the MiSeq illumina sequencing platform. *Appl. Environ. Microbiol.* **79**, 5112–5120 (2013).
50. Cole, J. R. et al. Ribosomal Database Project: data and tools for high throughput rRNA analysis. *Nucleic Acids Res.* **42**, D633–D642 (2013).
51. Wang, Q., Garrity, G. M., Tiedje, J. M. & Cole, J. R. Naïve Bayesian classifier for rapid assignment of rRNA sequences into the new bacterial taxonomy. *Appl. Environ. Microbiol.* **73**, 5261–5267 (2007).
52. Edgar, R. C., Haas, B. J., Clemente, J. C., Quince, C. & Knight, R. UCHIME improves sensitivity and speed of chimera detection. *Bioinformatics* **27**, 2194–2200 (2011).
53. Edgar, R. C. Search and clustering orders of magnitude faster than BLAST. *Bioinformatics* **26**, 2460–2461 (2010).
54. Edgar, R. C. UPARSE: highly accurate OTU sequences from microbial amplicon reads. *Nat. Methods* **10**, 996–998 (2013).
55. Wang, Q. et al. Xander: employing a novel method for efficient gene-targeted metagenomic assembly. *Microbiome* **3**, 32 (2015).
56. Tveit, A. T. et al. Widespread soil bacterium that oxidizes atmospheric methane. *Proc. Natl Acad. Sci. USA.* **116**, 8515–8524 (2019).
57. Grace, J. B. *Structural Equation Modeling and Natural Systems* (Cambridge University Press, 2006).
58. Lefcheck, J. S. piecewiseSEM: piecewise structural equation modelling in R for ecology, evolution, and systematics. *Methods Ecol. Evol.* **7**, 573–579 (2016).
59. Nakagawa, S. & Schielzeth, H. A general and simple method for obtaining R<sup>2</sup> from generalized linear mixed-effects models. *Methods Ecol. Evol.* **4**, 133–142 (2013).

## Acknowledgements

This project was funded by the Danish National Research Foundation (CENPERM DNRF 100). Sampling in North Greenland was made possible through the Mamont North Greenland expedition and the Leister Expedition around North Greenland. The portion of the study done in Michigan was funded by the US Department of Energy Office of Science, awards DE-SC0010715 and DE-FG02-99ER62848 and the U.S. National Science Foundation Awards DBI-1356380 and DBI-1759892. All the samples were collected and exported in agreement with the survey licence number G16-066 issued by the Ministry of Industry, Labour and Trade, Government of Greenland.

## Author contributions

B.E. conceived the study and collected all samples and together with L.D., J.R.C., K.K. and J.T. designed the experiments; L.D. was responsible for incubations together with J.R.C., samples preparation for chemical analyses together with P.W., data analyses and interpretation; B.B. was responsible for molecular analyses and interpretations with help from J.T.; Y.O. made the process-based modelling; S.K.R. made the SEM model; P.E.H. carried out the metal analyses; P.L.A. carried out the Total N and C analyses; K.K.B. was responsible for bioavailable Cu measurements and A.W.-N. for all climate data. L.D. compiled the main dataset, drafted the MS with input from B.E., J.R.C., B.B. and K.K.B., and finalised the MS after comments from all authors.

## Competing interests

The authors declare no competing interests.

## Additional information

**Supplementary information** The online version contains supplementary material available at <https://doi.org/10.1038/s43247-023-01143-3>.

**Correspondence** and requests for materials should be addressed to Ludovica D’Imperio or Bo Elberling.

**Peer review information** *Communications Earth & Environment* thanks Sari Juutinen, Xiaofeng Xu and the other, anonymous, reviewer(s) for their contribution to the peer review of this work. Primary Handling Editors: Joshua Dean and Clare Davis. Peer reviewer reports are available.

**Reprints and permission information** is available at <http://www.nature.com/reprints>

**Publisher’s note** Springer Nature remains neutral with regard to jurisdictional claims in published maps and institutional affiliations.



**Open Access** This article is licensed under a Creative Commons Attribution 4.0 International License, which permits use, sharing, adaptation, distribution and reproduction in any medium or format, as long as you give appropriate credit to the original author(s) and the source, provide a link to the Creative Commons license, and indicate if changes were made. The images or other third party material in this article are included in the article’s Creative Commons license, unless indicated otherwise in a credit line to the material. If material is not included in the article’s Creative Commons license and your intended use is not permitted by statutory regulation or exceeds the permitted use, you will need to obtain permission directly from the copyright holder. To view a copy of this license, visit <http://creativecommons.org/licenses/by/4.0/>.

© The Author(s) 2023